OPTIMIZATION OF A HYBRID RENEWABLE MICRO-HYDROPOWER WITH A PUMPED HYDRO ENERGY STORAGE SYSTEM

[1]EMILE NIRINGIYIMANA, [2]ZHANG PING, [3]WANG KEDONG, [4]CHEN HUIWEI

School of Intelligent Manufacturing, Qingdao Huanghai University
E-mail: nemile1988@gmail.com

Abstract - The integration of standalone renewable energy (RE) sources, such as hydropower and photovoltaics (PV), is crucial for achieving sustainable development goals. However, their intermittent and unpredictable nature poses a significant challenge to reliable capacity planning. This paper addresses this challenge by optimizing a hybrid RE system that synergizes a standalone PV array with a micro-hydropower station, using pumped storage as a critical energy storage solution. The proposed system aims to enhance overall energy production, ensure a reliable power supply, and meet the fluctuating demand of a local community. The ideal configuration, consisting of a 100-kW PV array and a 200-kW hydropower turbine, was optimized in HOMER Pro software to minimize the Net Present Cost (NPC), Cost of Energy (COE), and unmet load. The modified incremental conductance algorithm was employed for component sizing and selection. Validation in MATLAB/Simulink, using case study data, confirmed the system's feasibility. Results demonstrate that the PV array effectively complements the micro-hydropower during periods of low river flow, with the pumped energy storage ensuring consistent and reliable power delivery.

Keywords - Hybrid Power System, Hydropower Reservoir, PV Systems, Energy Storage with Pumped Storage, HOMER Optimization

I. INTRODUCTION

Due to the lack of accessible, dependable electricity, challenging terrain and environmental considerations, connecting remote areas to national grid is very challenging. These are significant obstacles to electrification development in rural areas. Renewable energy (RE) showed a huge trend as stated in the statistics report of 2019 that worldwide RE generation reached 2179 GW[1]. The largest portion of 1152 GW is occupied by hydropower, followed by solar energy (514 GW), wind energy (397 GW), biomass energy (116 GW), and geothermal energy (500 GW) as shown in Table 1.

REs showed the potential to be the alternative way to mitigate the power generation problems in many countries with critical development[2]. Among all the renewable energy sources, solar energy became popular since they offer a great opportunity to generate electricity while reducing greenhouse gas emissions[3].

No	Type of RE generation	Capacity (GW)
1	Hydropower	1152
2	solar energy	514
3	wind energy	397
4	biomass energy	116
5	geothermal energy	500

Table 1: Worldwide RE generation

In [4]authors stated that electricity from solar PV is inactive during the winter and night hours. PV was recognized as having the highest development potential due to its established technology, and competitive operating costs with other electricity generation systems and the most environmentally sound RE sources accessible to everyone[5]. Hybrid systems with battery backup was found more reliable with several benefits compared to standalone solar PV, hydropower, or wind alone [6]. Authors in [7] stated that suitable hybrid RE system satisfying the load demand, the power system reliability and cost effectiveness must be properly evaluated. Hydropower is effectively explored if they are properly designed and installed with accurate parameters setting and use of efficient devices[8]. In [9] authors addressed the optimal sizing and techno-economic study of a grid-connected PV-Pumped Storage Hydro-power Plant (PSHP) using an Improved Search Space Reduction (ISSR) algorithm. The multi objective genetic algorithm (MOGA) optimization technique in [10] was used to assess optimal size of hybrid solar PV, wind, and hydro energy system.

Solar irradiance in Rwanda is between 4-6 kWh/m2/day which is enough for PV panels to generate electricity[11] [12]. However, the conditions vary from season to season, with an average daily irradiation levels about 4.5 kWh/m² in the cloudy days with 66.8 TWh total annual potential estimation[13]. Due to the low investment in energy sector, there is no exploitation of this RE source and no feasibility study[11]. By 2022, the amount of electricity produced by power plants Rwanda was 332.6 MW, with 43.9% from hydro, 51% from thermal and 4.2% from. It is necessary to consider rural electrification using non-conventional energies such as hydro, solar, geothermal and wind. However,

the operation of each isolated power source may not be effective enough[14].

Mutobo is located in high latitudes with long-time available sunshine of 5.87 kWh/m2/day in the driest month of July and the temperature between 23~320C. Mutobo hydropower is near the area reserved for a special economic zone of about 80 Ha. Due to these factors, the development of hybrid plants with low-cost options ensures its future power supplies[15][16]. In order to deliver a secure, dependable, and high-quality supply to the demands, hybrid systems optimization places an emphasis on the selection of best components, the advanced methodology, and its sizing[17].

II. HYBRID SYSTEMS

In the past decade, researchers focused on the exploration of hybrid energy systems operation[18]. Hybrid systems are frequently used as the first option to provide reliable and sustainable electric power under various climate change scenarios. The complementary of RE systems compares economic and technical performances with conventional and fossil fuel power supply[19]. Hybrid RE systems varies from mini power supplies for remote areas[20].

a. RE potential in Rwanda

Rwanda has significant potential for RE, particularly hydropower, solar, and geothermal energy[21]. Hydropower is the most developed RE which makes up the larger part of the electricity generation due to its technological maturity. Solar energy has a great potential that led to the development of several solar projects, including the 8.5 MW solar power plant in Rwamagana District. Several areas in Rwanda could be suitable for geothermal energy with a potential of 300 MW [69] [70].

b. Utilization of RE in Rwanda

The recent increase of oil price combined with intermittent power outages and Rwanda's high electricity tariff are driving researches development in RE. The electricity price in Rwanda is the most expensive in East Africa with an average of US$0.25/kWh compared to US$0.15 in Kenya and US$0.17 in Uganda[22].

Hydro energy

In [23] authors suggested that country's topography makes micro-hydro and medium-hydro runoff river schemes as shown in table 2 the most suitable to meet the country's hydropower generation projected to be 500 MW by 2024. The latest total hydropower generation is 26.2MW in the north of Rwanda with 22.5MW from Ntaruka and Mukungwa power stations, and the rest is from Mukungwa II and Mutobo.

Plant name	River	Capacity
Ntaruka	Mukungwa	11.5MW
Mukungwa	Mukungwa	12MW
Mukungwa II	Mukungwa	2.5
Mutobo	Mutobo river	200KW
Rusumo	Akagera	80MW
Nyabarongo II	Nyabarongo	43MW
Rusizi III	Rusizi river	147MW
Rusizi IV	Rusizi river	287MW

Table 2: Hydropower plants available in Rwanda

Solar energy

Power station	Capacity	Location	Completed
Rwamagana solar	8.5MW	Rwamagana	2015
Ngoma solar	2.4MW	Ngoma	2011
Nasho solar	3.3MW	Rwinkwavu	2018
Jali solar	0.25MW	Kigali	2007
Ndera Solar	0.15MW	Kigali	2014
Gisozi memorial	0.2MW	kigali	2015
Ngoma solar	30MW	Ngoma	In process
Nyamata solar	0.003MW	Bugesera	2020

Table 3 Standalone and grid connected solar PV plants

According to NASA records; in June, July, and August the highest solar radiation is received with solar radiation
ranging between 4.3 and 5.2 kWh/m2/day [76].

III. METHODS

a. Area selection

An unelectrified Mutobo located between 02028′06" S 29033′12″E in Northern of Rwanda was selected. Figure 1 shows the Mutobo man-made micro upper reservoir and the site under construction of 200kW where (1) is the water intake, (2) De-silting bay, (3) Canal, (4) micro upper reservoir, (5) Penstock and (6) Powerhouse.



Fig 1. Mutobo micro power Plant with upper reservoir

b. Data collection

Solar, wind, geothermal and biogas are few of the new energy sources that could be developed in this area.

Through the use of latitude and longitude, HOMER principles were used to calculate the daily solar irradiation, wind speed, and ideal system sizing. Different loads with 300 households 2 schools and 1 health center are recorded in this project.

The specifications of the PV panels used in the system design was selected from the HOMER software and the micro-hydropower components specifications such as the penstock of 223m, the reservoir elevation of 1550m, the yearly generation of 1749.8Mwh, turbine efficiency of 65% and the flowrate of 0.932 m3/s.

Table 4 shows the weather data collection throughout the year from meteorological data observatory located between $02^0 28' 06"$S and $29^0 33' 12"$E[26]

Month	Clearness index	Radiation kwh/m²/day	Wind speed ms⁻	Air t°(°C)	Rainfall (mm/month)	Runoff depth(mm/month)	Atm pressure kPa	Relative humidity (%)
Jan	0.532	4.47	3.8	21	83	50	89.7	43.30%
Feb	0.531	5.59	3.9	21.1	88	55	89.7	44.50%
Mar	0.531	5.19	3.9	21.1	142	79	89.6	62.60%
Apr	0.502	5.07	3.7	20.6	158	84	89.7	75.00%
May	0.527	4.98	3.6	20.5	110	61	89.8	75.50%
Jun	0.597	5.41	3.5	20.8	21	15	89.9	68.70%
Jul	0.638	5.87	3.5	20.9	10	5	90	62.20%
Aug	0.586	5.72	3.5	21.5	31	18	90	69.70%
Sep	0.551	5.68	3.6	21.2	79	42	89.9	75.20%
Oct	0.529	5.53	3.7	21.1	122	65	89.8	78.10%
Nov	0.485	4.99	3.6	20.2	139	78	89.8	72.70%
Dec	0.5	4.8	3.6	20.5	110	60	89.8	54.80%

Table 4: Monthly meteorological data observatory for Mutobo village

Load profile overview and Energy demand estimation Hydropower stations are affected by seasons variation considering the flowrate from June to August due to twice-yearly passage of the Intertropical Convergence Zone[28]. According to [29] report of 2020 more than 52.2% of Rwandans have access to energy with 38% via grid connection and 14% off-grids. The government has access to a variety of indigenous energy sources that could complement each other to adopt standalone hybrid RE as alternative energy for the future energy [30]. The most practical ressources includes PVs, hydro, biomass, peat, methane gas and geothermal[22].

Appliance	Rating (W)	qty	hrs/ day	demand kWh/day)
Bulbs	30	8	4	2.08
Electric fan	80	5	8	5.20
Fridge	150	1	24	3.60
TV	150	1	5	0.75
Microwave	2100	1	0.5	1.05
Rice cooker	650	1	2	2.30
Blender	400	1	0.5	0.2
mobile	10	3	2	1.06
Grand total				11.24

Table 5: Load requirements for a single household

The hydro power supply is 47% of the total power generated [31] [32]. In the north province the main energy demand includes home and street lighting and forecasting the future load demand of Musanze industrial zone area.

The daily average energy consumption is 1.4 kWh, with a maximum load of 15 kW based on electricity consumption record from the 200 households, one hospital, and one school, as well as personal power ratings of domestic devices as shown in Table 5.

a. Optimization framework

Different softwares have been developed for analyzing hybrid system such as HOMER, RET Screen, PVsyst, Hybrid2 etc. HOMER is the most popular tool for sizing hybrid systems, simulating various power plant systems, and optimization identify the best power plant configuration in terms of operating costs, NPC, gas emissions, and economic comparison and performs complex optimization task precisely by doing hourly simulations of the power flow between load and other components[33][34].

Component	Characteristics	value
PV module	Nominal power (Ppv)	327W
	Panel efficiency(ηpv)	21.45
	Rated voltage (Vmpp)	54.7v
	Rated current (Impp)	5.98A
	Open circuit voltage (Voc)	64.9V
	Short circuit current (Isc)	6.46A
	Power temperature coefficient(αp) NOCT	-0.35%/oC 45oC±2 oC
Inverter	Rated power (Pinv)	20Kw
	Conversion η_{inv}	95%
Pump-hydro	Nominal capacity (Pphs)	22kw
	Net head(h)	30m
	Round trip efficiency(ηphs)	70%
	Reservoir capacity (Rc)	4280m³

Table 6: Technical parameters of components

Technical characteristics, economic data of different components such as PV module unit, inverter, pump-hydro specification are introduced in the HOMER optimization tool and presented in Table 6.

Electric loads, solar irradiance, hydro resources, component parameters and costs are used as inputs[35]. The PV size, turbines output, inverters size, and batteries are variables in Homer's performance.

The best optimal model configuration satisfies the requirements at the lowest total NPC[36]. HOMER's optimization and sensitivity analysis algorithms evaluates the economic and technical viability of numerous technological options while accounting for changes in technology costs and the availability of energy resources.

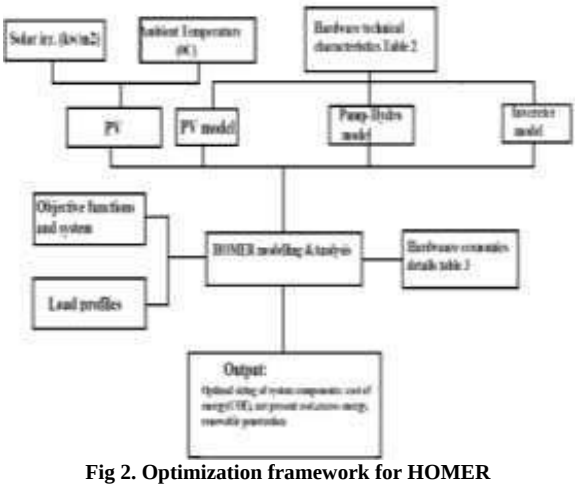

Fig 2. Optimization framework for HOMER

The hybrid solar PV-hydropower system comprises two power sources: solar PV panels and hydro turbines and storage option to provide an optimized system efficiency and more balanced power supply[37].

Due to the unpredictability and discontinuous of solar, the hybrid systems do not only need to exploit the maximum efficiency of the power generated, but also needs to balance the stability of the grid output [38]. The figure 3 shows the overview of RE sources distribution.

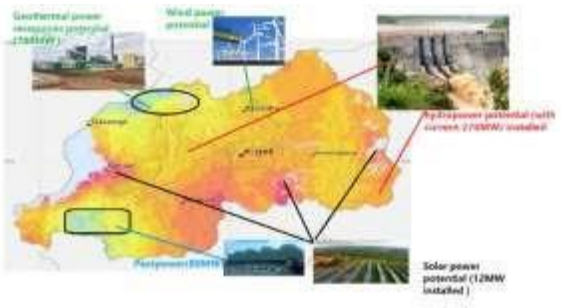

Fig 3. RE resources distribution

IV. SYSTEM MODELING

a. PV system modelling

The intermittent nature of solar irradiance stands in the way of using solar energy as the single energy source of standalone systems[39]. The location of the PV array, including variations of solar intensity, temperature, tilt angle, and wind speed, has an impact on power output of the PV panels and the cooling effect of wind speed on PV panels is significant in windy areas[40].

PV cell operation

In PV installation, the PV cell is the smallest component that converts light energy into electrical energy. It is only based on a semiconductor p-n junction diode that functions when illuminated by sunlight[41].

PV array system description

The PV array system is made of 20 parallel module strings and 15 series-connected 305.2-W solar panels which has a maximum power output of 100kW at STC (800 W/m2, 250C). A DC-DC boost converter, a three-level voltage source converter (VSC), and a step-up transformer that adjusts the AC power from the voltage source converter are utilized to connect the output from solar PV array to the transmission system. A modified incremental conductance MPP is used in the boost converter to implement the Maximum Power Point Tracking (MPPT).

Factors influencing the PV cell operation

The generated current from the solar cell is calculated using the fundamental equation 1. The figure 4 shows the array system with modules connected together in series and parallel connection.



Fig 4. PV array system

The figure 5 shows the variation of the short-circuit current (Isc) linearly with solar radiation, while the voltage remains relatively unchangeable. Although temperature has a negligible impact on current, it has a negative impact on open-circuit voltage[42].

$$\mathbf{I} = I_L - I_o\,[Exp\{\frac{q(V+IR_s)}{akT}\} - 1] - (V + IR_s)/R_{sh} \quad (1)$$

Where I: Cell O/P current, Ip: Photocurrent, Id: saturation current, q: Electron charge (1.6 e19 C), V: PV cell output voltage, Rs: Series resistance, K: Boltzmann's constant (1.38 e23 J/K), T: Temperature (K), N: Ideality factor (1~2), Rsh: Parallel resistance, The photocurrent is calculated in Equation 2 [43] depending on solar irradiance and cell temperature.

$$I_p = -I_{sc} + K_t(T_c - T_r) \times \frac{Hr}{1000} \quad (2)$$

Where: ISC: Short circuit current, Ki: to coefficient, TC: Cell temperature at STC, Tr: Cell Ref to at STC, Hr: Solar Irr in W/m2

The PV model is modeled from equations 1 and 2, and the total output power is calculated by equation 3. The I-V and P-V characteristics curves in Figure 5 are extracted at various levels of solar irradiance.

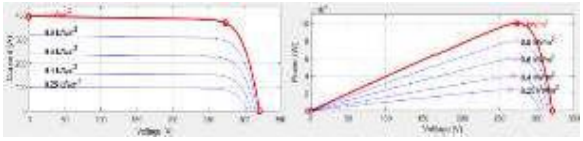

Fig 5. Behaviors of the PV parameters at different solar radiation (a)I-V (b) P-V

Some PV strings must be connected in parallel when a large amount of current is needed in the system[44]. Several parameters, including solar radiation on the PV panel surface Gβ(w/m2), PV operating temperature (T0) in oC, inverter efficiency (ηinv) in %, and losses (ηloss) in %, regulate the power generated by PV modules.

$$P_{PV} = \eta_{PV} A_{PV} G_{\beta} \quad (3)$$

$$\eta_{PV} = \eta_{Inv} \eta_{loss} \eta_{ref} [1-k(T_o - T_{ref})]$$

$$P_{PV} = [\eta_{inv} \eta_{loss} \eta_{ref} (1-k(T_0 - T_{ref}))A_{PV} G_{\beta} \quad (4)$$

Where P_{pv} is the power output from the PV panels, η_{pv} is the efficiency, A_{pv} is the area of PV panels, G is the solar radiation intensity, η_{ref} is the module reference efficiency in % under the reference temperature 25 0C (T_{ref}), k is the temperature coefficient and A_{pv} is the area of the PV array(m2). The reference parameters of the PV modules used in this research includes; the reference efficiency(η_{ref}) of 0.95, the inverter efficiency(η_{inv}) of 0.12, loss efficiency (η_{loss}) of 0.86 and temperature coefficient (K) of 0.004.

Solar radiation on tilted PV surfaces

To improve performance, the PV panels will be angled with respect to the horizontal plane. Beam, diffuse, and ground-reflected solar irradiances are the three main determinants of the total amount of radiation that the PV panel extracts. Equation 5 estimates the irradiation on tilted PV surfaces:

$$G_{\beta} = G_{\beta,b} + G_{\beta,d} + G_{\beta,r} \quad (5)$$

Where: G_{β}: total radiation (W/m^2), G_{β}, b: direct beam, $G_{\beta,d}$: diffuse and $G_{\beta,r}$: ground reflected irradiance(W/m2) Three constituent terms are defined as follows:

Beam radiation $G_{\beta,b;}$

$$G_{\beta,b} = G_b \frac{\max(0,\cos\theta)}{\max(0.087,\cos\theta_z)} \quad (6)$$

Where G_b: horizontal direct radiation (W/m^2), θ: incident in degrees and θ_z: zenith angle in degrees The diffuse radiation;

$$G_{\beta,d} = G_d .[(1-F_1).(\frac{1+\cos\theta}{2}) + F_1 \frac{\max(0,\cos\theta)}{\max(0.087,\cos\theta_z)} + F_2 \sin\beta] \quad (7)$$

G_d: horizontal diffuse radiation, and β: the tilt angle The F_1 and F_2 coefficients, which represent the sky clearness and brightness indices, respectively, are degrees of circumsolar and horizon anisotropy.

The radiation reflected off of the ground;

$$G_{\beta,r} = \varepsilon(G_b + G_d).(\frac{1-\cos\beta}{2})$$

Where ε= 0.2 is the constant albedo in this work.

PV module temperature

The accurate Equation 8 [45] estimates the temperature on PV modules taking into account the wind speed.

$$T_c = T_a + (\frac{0.32}{8.91+2.0V_f})G_T \ (V_f > 0) \quad (8)$$

Where: T_a: surrounding air temperature (^{o}c), G_T irradiance on module plane (W/m^2), T_c: operating temperature and V_f: wind speed (m/s).

$$V_f = V_{ref}^{*} (\frac{Z_{pv}}{Z_{ref}})^n$$

$$n = \frac{0.37-0.088\ln(V_{ref})}{1-0.088\ln(z_{ref}/10)}$$

Where z_{pv} is the PV installation height (m). z_{ref} and V_{ref} are the reference height relative to ground (m) and wind speed at the reference height (m/s), respectively.

Modified incremental conductance algorithm

The algorithm uses the derivative of PV panel's voltage with respect to its current dV/dI, determining the MPP. The algorithm in Figure 6 compares the incremental conductance of the current operating point with that of the adjacent points on the power-voltage curve.

From the basic relation 9 below; Where I&V are the panel's terminal current and voltage; whereas dI and dV are fundamental components of I and V ripples. The integral regulator minimizes the error $\frac{dI}{dV} + \frac{I}{V}$ so that the regulator output the duty cycle correction.

$$P = VI \quad (9)$$

$$\frac{d(V \times I)}{dV} = I + V\frac{dI}{dV} = 0$$

The conditions for the true MPPT on the PV curve are;

$$\frac{dI_{pv}}{dV_{pv}} = 0 \; ; \; I + V\frac{dI}{dV} = 0 \qquad \text{Then,}$$

$$\frac{dI}{dv} = -\frac{I}{V}$$

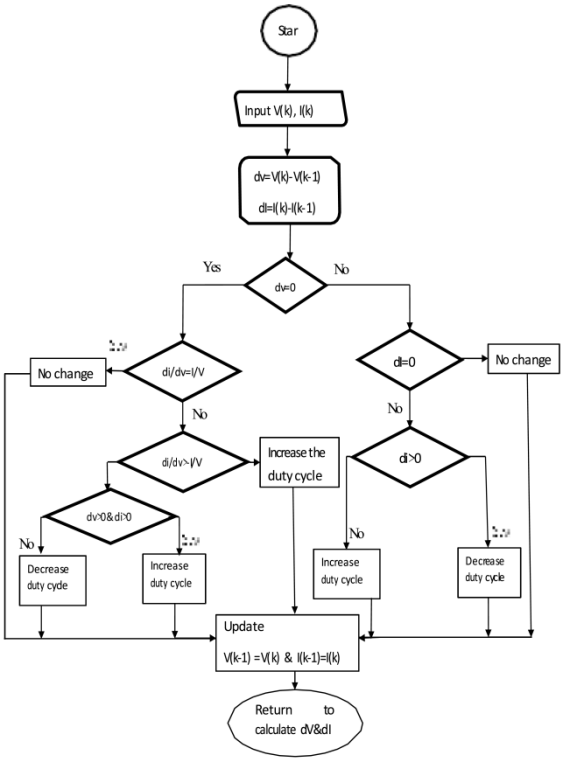

Fig.6 Modified Inc. Conductance algorithm

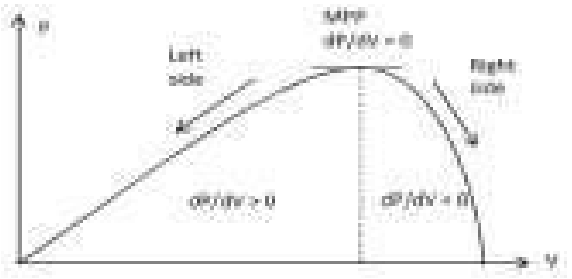

Fig.7 Principles of the Inc. Cond. algorithm

To obtain the maximum power output from the PV panels, the modified incremental conductance algorithm in Figure 7 explores these requirements by using a controller. If the incremental conductance of the current point is equal to the adjacent point, then the current point is the MPP. However, if the incremental conductance is greater or less than that of the adjacent point, the algorithm adjusts the operating point in the appropriate direction until it reaches the MPP.

b. Hydropower

Equation 10 estimates the output from the turbine;

$$P_{hyro} = \eta_{hydro} \times P \times g \times Q \times H \qquad (10)$$

Where P_{hydro} is the output of turbines, η_{hydro}: efficiency, ρ: density of water, g is the acceleration due to gravity, Q is the water flow rate, and H is the head of water. The nominal power generated is obtained from equation 10.

$$P_{hyd,nom} = \frac{\eta_{hyd} \times \rho_{hyd} \times g \times H \times Q_{design}}{1000} \qquad (11)$$

Hence, the total power generated from the hybrid solar PV-micro hydropower is obtained from equation 12.

$$P_{total} = P_{pv} + P_{hydro,nom} \qquad (12)$$

Hydropower station with pumped-storage installation model

The Hydropower station with pumped-storage installation model The hydrological data clearly showed that the chosen location experienced a water discharge in dry seasons. Additionally, the hydrological year's stream flow rate ranged from 0.733 m^3/s to 1.1 m^3/s, with an average annual stream flow of 0.932 m^3/s.

The upper and lower reservoirs, the variable speed pump, water turbine, and hydropower station with pumped storage installation are all crucial components. The upper reservoir of the hydropower plant receives continuous water from the natural inflow, and any extra energy produced by the PV modules is stored as the gravitational potential energy of the water. When PV outputs a small energy (EPV) than the energy demand of the local load (Eload), the system requires the discharge of some water from the upper reservoir to generate adequate electricity to compensate the missing power to supply the load. An additional variable energy (E_{add} in kWh) in Equation 13
[46] expresses the surplus energy.

$$E_{add} = E_{pv} - E_{load} \qquad (13)$$

When solar is not present during the day or night, the HSPSI should be able to meet load. When solar energy is abundant, the excess is used to pump water from the lower reservoir to the upper reservoir. When the reservoir is in cubical form, its capacity in (m3) is expressed in 14.

$$V_M = abh \qquad (14)$$

Where; ‘a’ is the length and ‘b’ is the width of upper reservoir in (m) and H is the height of the dam (m).

The changing water volume in the reservoir can be represented mathematically in equation 15.

$$V_A = V'_A + Q_{river} + Q_{P,T} \quad (15)$$

Where V'A is the present water quantity from the previous hour in the upper reservoir (in m^3). Qriver represent the natural inflow to the upper reservoir (m^3/h). The positive value of $Q_{P,T}$ (m^3) means the water is pumped from the lower reservoir to the upper reservoir and when it is negative it means the water is released from the upper reservoir.

The charging capacity and discharging capacity of HSPSI hybrid energy systems are primarily determined by variable-speed pump and water turbine. Water turbine and variable-speed pump under sizing increases the risk of the load loss and results in energy waste. When the water turbine and the variable speed pump are oversized, it increases the cost and decreases efficiency of the system. Capacity of released water;

$$Q_{dis} = \frac{E_T}{\eta_{T\rho g}\left(\frac{V'_A}{ab} + H\right)} \quad (16)$$

$$E_T \min\left(\frac{V'_A}{3600}, Q_T\right)\eta_T \rho g\left(\frac{V'_A}{ab} + H\right) \quad (17)$$

Where: E_T (kWh) is the energy generated by the water turbine at each hour when the quantity of released water is Qdis (m^3), Q_T: water turbine throughput (m^3/s), H: the basic hydropower height, ηT: overall efficiency of the water turbine (%), P: water density (1000 kg/m^3), G: gravitational acceleration (m/s^2).

The water released from the reservoir cannot exceed the water from turbine and the water left in upper reservoir. Every hour, the height is updated because the water level in the upper reservoir changes when the water turbine or variable-speed pump is running. The pumped water from the lower reservoir to the upper reservoir can be calculated by the equation 18.

$$Q_{pump} = \frac{\eta_p E_T}{\rho g\left(\frac{V'_A}{ab} + H\right)} \quad (18)$$

$$E_p = \min\left(\frac{V_M - V'_A}{3600}; Q_p\right)\frac{1}{\eta_p}\rho g\left(\frac{V'_A}{ab} + H\right) \quad (19)$$

Where: E_P (kWh): energy used per hour by the variable-speed pump to pump water quantity Q_{pump} (m_3). Q_P: variable-speed pump amount (m_3/s), η_P: overall efficiency of the variable-speed pump (%).

c. Proposed system model

The hybrid system configuration in figure 9 consists the hydro turbine, the upper and lower reservoir, the PV array system, DC-DC boost converter, the DC bus, the DC/AC converters and an MPPT. The three level, neutral point connection inverter is used as PV-hydro grid system power electronic interface. The boost converter and VSC converters are represented by equivalent voltage sources generating the AC voltage averaged over one cycle of the switching frequency.

In microgrids dynamic systems, several variables can be changing continuously due to different system operating conditions[47]. The design and simulation are performed in HOMER for the system technical performance optimization and economic viability.

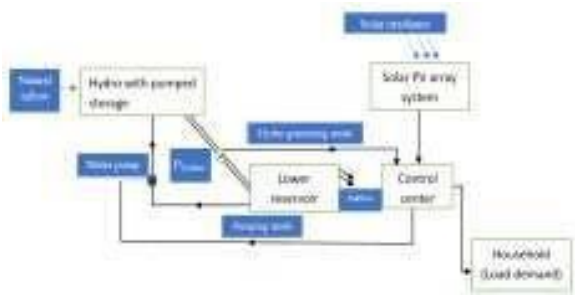

Fig.8 System block diagram of the proposed hybrid PV-micro hydropower generation model

Hydro Pumped storage system configurations

Hydro Pumped Storage (HPS) systems typically consist of two reservoirs. During periods of low energy demand, water is pumped from the lower reservoir to the upper reservoir. When energy demand increases, water is released from the upper reservoir and drives turbines. The pumped storage configuration depends on factors, such as location, available topography and energy demand. The pumped storage parameters include; the power capacity of 1MW, pump efficiency of 70% and the initial volume of the upper reservoir of 100m3.

Solar PV array configuration

The PV installation arrangement is determined by project specific requirements and limits show in Table 7.

No	Components	Rating capacity	unit
1	PV array (at STC; 800 W/m^2, 25^0 C)	100	kW
2	1980-Hz 3-level 3-phase	273 Vdc to 500 Vdc,	Volts
3	Inverter	20	kW

Table 7: Solar PV array configuration

The system dynamic modelling consists a PV array of 66 parallel strings and 5modules delivering a maximum of 100kW at STC (800 W/m^2, 25^0 C), a 5-kHz DC-DC boost converter and 3-level 3-phase voltage source converter (VSC). The designed PV system has a capacity to generate 100kW power using SunPower modules (SPR-305E-WHT-D) with the system boost converter parameters. The duty cycle and the DC-DC boost converter are obtained by solving equation 20.

$$D=1-\frac{V_{in}(min)\times\eta}{V_o} \quad (20)$$

$$V_0=\frac{V_{in}(min)\times\eta}{1-D}$$

$$1-D=\frac{V_{in}(min)\times\eta}{V_0}$$

Where; V_{in}: Input voltage, V_o: output voltage, Ƞ: Converter efficiency

V. SIMULATION RESULTS

From the model simulation the figure 9 showed the pumped storage hourly inflow measured in m3/s. This figure demonstrates that water is pumped back into the upper reservoir from the turbine outlet during the active hours of 6am to 5pm. When solar irradiance is high enough to generate electricity, with the maximum pumping capacity occurring between 10am and 4pm, when the pumping capacity reaches 0.35m3/s.

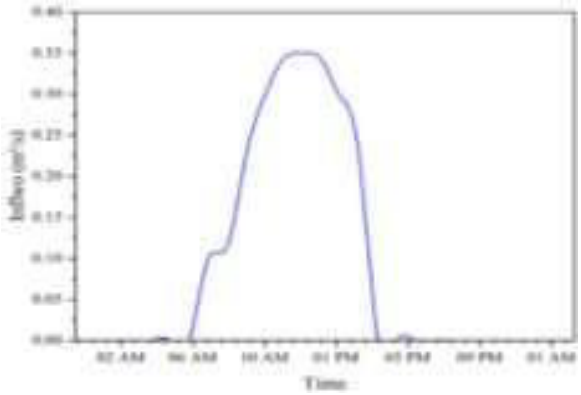

Fig.9 Hourly water inflow to the pumped storage in m^3/s

The monthly system pumped Load from January to December is shown in Figure 10. From the figure it is shown that from June to September the pumped load is high reaching up to 0.275MW.

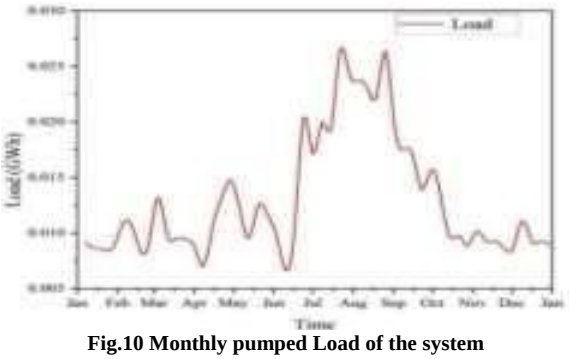

Fig.10 Monthly pumped Load of the system

From Figure 11 the monthly pumped water throughout the year is shown. The solar radiation is high from July to October which is obvious that the quantity of pumped water is also high reaching 70.000m^3.

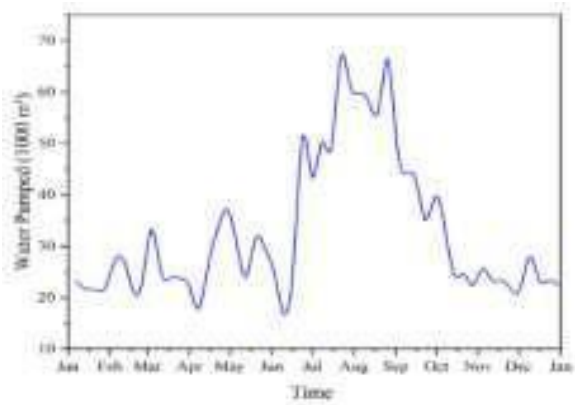

Fig.11 Monthly pumped water throughout the year

From simulation, the periodical system production in May and July are presented on Figures 12(a) and (b). The hydropower daily production in May is high during the night raising the generation to 0.16MW and the PV array day production is active from 6am to 4pm during the day when the irradiance is at maximum in May. From Figure 12(b), the hydropower system production in July is less than that of the PV array. The PV module day production can reach up to 0.35MW during the day between 8am to 4pm. This demonstrates that the solar system can complement the hydropower system during the dry season to overcome the reservoir water deficit which results in the energy production decrease. The average daily energy demand of the system is 165.44kWh which gives the monthly demand for the rural communities in Mutobo equals to 4963.2 kWh and yearly demand of 59.558 MW.

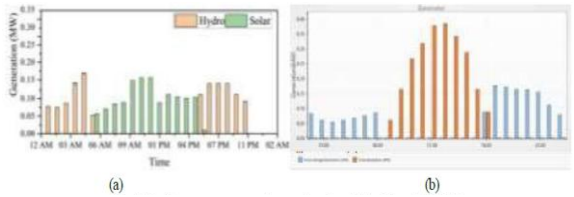

Fig.12 Daily system generation production: (a) in May (b) in July

From figure 13 it is obvious that solar PV array energy generation is abundant during summer season in June, July, and August, when hydropower production is reduced due to the decrease of reservoir water level. As a result, the production from solar generation can help to offset this energy crisis caused by the dry season. In July, hydropower generation falls to 150 kW, while energy produced by PV modules increases over 100 kW, depending on the amount of irradiance striking the solar module.

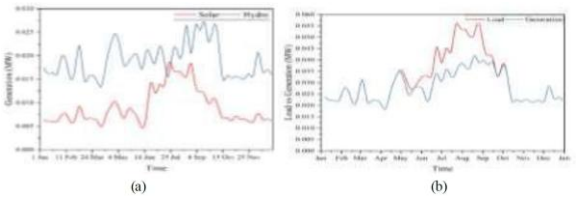

Fig.13 Yearly generation: (a) PV array and hydropower (b) Load vs generation in (MW)

The Figure14(a) shows a 24hours day production in July from pump storage vs solar generation from mid-night to 10pm of the day. The generation from solar is high during the day due to high uniformity of the irradiation profile throughout the day and the good match between production and consumption. From figure 14(b) the relation between the generated power capacity and load demand in MW from January to December is shown. The load demand is higher than the production in June, July, August and September.

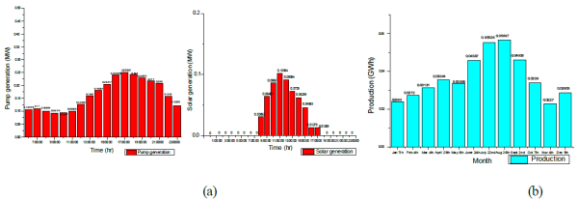

Fig 14. System production (a) in July (b) maximum production from Jan- Dec

VI. SYSTEM VALIDATION IN MATLAB

The solar irradiance at standard testing condition (STC) is 1000 W/m2 at 250C. The duty cycle is constant from time t=0 sec to t= 0.3 sec (D= 0.5). The output voltage is calculated by using V= (1-D) *Vdc. The mean array output power is 96 kW whereas specified maximum power generated at STC is 100 kW. The MPPT is enabled at time t=0.3sec, therefore the MPPT regulator starts regulating the PV voltage by varying the duty cycle in order to extract the maximum power generated from the PV.

The maximum power is obtained at the duty cycle D=0.453. From time t=0.3 sec to 0.5 sec, the array operates at STC, the duty cycle varies between 0.450 and 0.459. The PV array generation are calculated from equations 21 and 22.

$$V_{PV} = N_{ser} \times V_{mp} \quad (21)$$

VPV=5x54.7=273.5V, this voltage is later regulated to 500V in figure 16 by varying the duty cycle.

$$P_{PV(out)} = V_{PV} \times I_{PV} \quad (22)$$

$$P_{PV(mean)} = 273.5 \times (66 \times 5.58)$$

PPV (out)=100.7kW, as expected from PV array simulation in Figure 15.

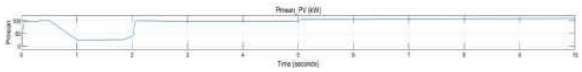

Fig.15 PV array output power

When the irradiance is ramped down from 0.5 to 1 sec, from 1000 to 250 W/m2, the MPP controller tracks maximum power only while irradiance stays constant. When the irradiance stays at 250 W/m2 and the duty cycle value increases from 0.466 to 0.473, the PV voltage and power also decrease to 265V and 24.4kW respectively. From t=1.5 sec to t=6.0 sec sun irradiance is restored back to 1000 W/m2 and then temperature is varied between 20 and 50C. This shows the impact of temperature on the output of the PV module when environment condition changes especially temperature and irradiance. The desired maximum PV output (107.5 kW) is obtained from the 2sec to 10 sec when irradiance is at maximum and when temperature is decreased to 50C. Vref-Vmean output of the DC-DC converter are shown in Figure 16 which converges more rapidly to MPP between 0.5sec to 1sec interval when irradiance decreases compared to traditional incremental conductance algorithm. from the figure 17, the system voltage and current are in phase with the value of 400V and 5A respectively.

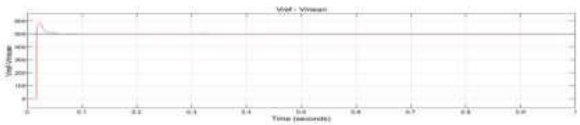

Fig 16. DC-DC boost converter Output voltage

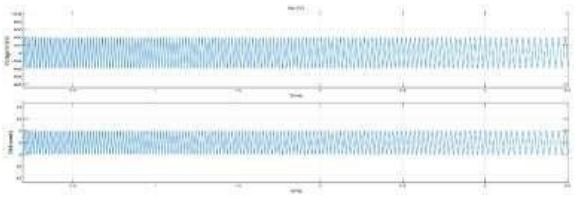

Fig.17 System outputs (voltage and current)

VII. CONCLUSION

Hybrid RE systems hold promise as a reliable and continuous source of power for remote areas that alleviate electricity shortages, particularly in rural areas. For low power generation during dry seasons, modeling and optimization of hydropower reservoir using hybrid RE systems are helpful. This work developed the prospect and cost effectiveness hybrid system complementarity between a 100kW standalone PV system and a hydropower station with a pumped storage reservoir in for Mutobo village. In order to establish the optimal hydropower reservoir using RE system with adequate sizing of system components, electricity demand, solar radiation, hydrology, climate data were used as system input. The average daily solar radiation is 5.6 kWh/m2 and

average wind speed is 3.5 m/s in Mutobo. The ideal integrated RE system, according to HOMER optimization, consists of 91.21kW from PV at the lowest solar irradiance and 146kW from micro-hydropower at the minimum flowrate has been achieved. The developed approach optimal sizing study is carried out with incremental conductance algorithm for its fast-tracking ability with the fast variation of solar irradiance compared to another optimization algorithm such as perturb and observe (PO) algorithm.

Finally, the system was validated in Matlab and results showed the feasibility and applicability of the system. It is concluded that the system is a feasible and scalable solution for fulfilling the future energy demand in the in Mutobo village, and the suggested method successfully executes the considerable cost-effective solution without any environmental impact.

PROJECT FUNDING

This project was funded by the Qingdao Huanghai university Doctors startup funds.

REFERENCES

[1] X. Xu, W. Hu, D. Cao, Q. Huang, C. Chen, and Z. Chen, "Optimized sizing of a standalone PV-wind-hydropower station with pumped-storage installation hybrid energy system," Renew. Energy, vol. 147, pp. 1418–1431, 2020.

[2] A. Abubakar, "The Application of Homer Optimization Software to Investigate the Prospects of Hybrid Renewable Energy System in Rural Communities of Sokoto in Nigeria," Int. J. Electr. Comput. Eng., vol. 7, no. 2, pp. 596–603, 2017.

[3] C. I. Hoarcă, "On the energy efficiency of standalone fuel cell / renewable hybrid power sources Part II : Simulation results for variable load profile with different renewable energy sources profiles (RES)," 9th Int. Conf. Power Electron. - ECCE Asia "Green World with Power Electron. ICPE 2015-ECCE Asia2018 IEEE, pp. 2–6, 2018.

[4] W. Yuan, Z. Liu, C. Su, and X. Wang, "Photovoltaic capacity optimization of small and medium-sized hydro-photovoltaic hybrid energy systems considering multiple uncertainties," J. Clean. Prod., vol. 276, p. 124170, 2020.

[5] L. Lakatos, "Advantages and Disadvantages of Solar Energy and Wind-Power Utilization Advantages and Disadvantages of Solar Energy and Wind-Power Utilization," World Futur. J. Glob. Educ. ISSN, no. August 2011, 2020.

[6] B. D. Vick and B. A. Neal, "Analysis of off-grid hybrid wind turbine / solar PV water pumping systems," Sol. Energy, vol. 86, no. 5, pp. 1197–1207, 2012.

[7] P. Zhou, R. Y. Jin, and L. W. Fan, "Reliability and economic evaluation of power system with renewables : A review," Renew. Sustain. Energy Rev., vol. 58, pp. 537–547, 2016.

[8] H. S. Das, A. H. M. Yatim, C. Wei, and K. Y. Lau, "Proposition of a PV / tidal powered micro-hydro and diesel hybrid system : A southern Bangladesh focus," Renew. Sustain. Energy Rev., vol. 53, pp. 1137–1148, 2016.

[9] A. Bhimaraju, A. Mahesh, and J. S. Nirbheram, "Feasibility study of solar photovoltaic/grid-connected hybrid renewable energy system with pumped storage hydropower system using abandoned open cast coal mine: A case study in India," J. Energy Storage, vol. 72, no. July, 2023.

[10] A. S. Irshad et al., "Resilience and reliable integration of PV-wind and hydropower based 100% hybrid renewable energy system without any energy storage system for inaccessible area electrification," Energy, vol. 282, no. August, p. 128823, 2023.

[11] H. Eustache, D. Sandoval, U. G. Wali, and K. Venant, "Current Status of Renewable Energy Technologies for Electricity Generation in Rwanda and Their Estimated Potentials," Energy Environ. Eng., vol. 6(1):8-15, 2019.

[12] J. D. D. Uwisengeyimana, A. Teke, and T. Ibrikci, "Current Overview of Renewable Energy Resources in Rwanda Current Overview of Renewable Energy Resources in Rwanda," J. Energy Nat. Resour., no. October 2020, 2016.

[13] M. Asinyaka and J. Uwibambe, "Let There Be Light : Electrification Of Rural Communities In Rwanda Using Solar Pv Systems .," pp. 1–22.

[14] S. Ashok, "Optimised model for community-based hybrid energy system," vol. 32, pp. 1155–1164, 2007.

[15] F. F. Li and J. Qiu, "Multi-objective optimization for integrated hydro-photovoltaic power system," Appl. Energy, vol. 167, pp. 377–384, 2016.

[16] B. H. Wijaya, R. K. Subroto, K. L. Lian, and N. Hariyanto, "A maximum power point tracking method based on a modified grasshopper algorithm combined with incremental conductance," Energies, vol. 13, no. 17, 2020.

[17] J. B. Fulzele and S. Dutt, "Optimium Planning of Hybrid Renewable Energy System Using," vol. 2, no. 1, pp. 68–74, 2012.

[18] H. Su, H. Wei, X. Wei, G. Wang, Y. Zhang, and R. Wang, "Long-Term Optimal Operation of the Cascade Hydro-Wind-Photovoltaic Hybrid System considering Transmission Section Constraints," Math. Probl. Eng., vol. 2023, pp. 1–15, 2023.

[19] Z. Yang et al., "The complementary management of large-scale hydro-photovoltaic hybrid power systems reinforces resilience to climate change," J. Hydrol., vol. 612, no. PB,p. 128214, 2022.

[20] H. El and M. Al, "Comparison between hybrid renewable energy systems in Saudi Arabia," J. Electr. Syst. Inf. Technol., vol. 2, no. 1, pp. 111–119, 2015.

[21] M. C. Mukeshimana, Z. Y. Zhao, and J. P. Nshimiyimana, "Evaluating strategies for renewable energy development in Rwanda: An integrated SWOT – ISM analysis," Renew. Energy, vol. 176, pp. 402–414, 2021.

[22] S. Bimenyimana, G. N. O. Asemota, and L. Li, "The State of the Power Sector in Rwanda : A Progressive Sector With Ambitious Targets," Energy Syst. Policy, J. Front. Energy Res., vol. 6, no. July, 2018.

[23] E. Mudaheranwa, Y. Udoakah, and L. Cipcigan, "Rwanda ' s Energy Profile and Potential Renewable Energy Resources Mapping toward Sustainable Development Goals," in 2019 IEEE PES/IAS PowerAfrica, 2021, no. August 2019, pp. 1–5.

[24] E. Mudaheranwa, Y. Udoakah, and L. Cipcigan, "Rwanda ' s Energy Profile and Potential Renewable Energy Resources Mapping toward Sustainable Development Goals," in 2019 IEEE PES/IAS PowerAfrica, 2019, pp. 1–5.

[25] J. B. N. and V. N. Yongli, Wang, "Renewable energy access in Rwanda : Electricity Price Forecasting," in 2020 IEEE PES/IAS PowerAfrica, 2020, vol. 189, pp. 1–5.

[26] H. G. Beyer, "Design of Photovoltaic System for Rural Electrification in Rwanda by Jeannine Uwibambe Supervisor :," 2017.

[27] E. Niringiyimana, S. Wanquan, and G. Dushimimana, "Feasibility Study of a Hybrid PV / Hydro System for Remote Area Electrification in Rwanda," J. Renew. Energy, vol. 2022, 2022.

[28] H. Hubert and A. Maniragaba, "Effects Of Water Variation On Hydropower Plant Functionality A Case of Ntaruka Hydropower," East African J. Sci. Technol., vol. 7, no. January, pp. 39–52, 2017.

[29] M. Fidele and U. Ndahimana, "Investment Opportunities in the Rwandan Energy Sector," kingdom of Netherlands, 2020.

[30] E. Mudaheranwa, Y. Udoakah, and L. Cipcigan, "Rwanda ' s Energy Profile and Potential Renewable Energy Resources Mapping toward Sustainable Development Goals," in 2019 IEEE PES/IAS PowerAfrica, 2019, pp. 3–8.

[31] E. Hakizimana, D. Sandoval, U. G. Wali, and K. Venant, "Inventory Analysis Of Power Plants In Rwanda And Estimated Generation Capacities," Int. J. Sci. Technol. Res., vol. 9, no. December, 2020.

[32] E. Mudaheranwa, G. Masengo, Y. Odoakah, L. Cipcigan, and C. E. Ugalde-loo, "Development of Rwanda ' s Future Energy Scenarios for Long-Term Investment and Planning," in 2021 The 3rd Asia Energy and Electrical Engineering Symposium Development, 2021, pp. 1124–1129.

[33] L. Khalil, L. Khalil, K. Liaquat, M. A. Iqbal, M. Riaz, and K. Khalil, "Optimization and designing of hybrid power system using HOMER pro Materials Today : Proceedings Optimization and designing of hybrid power system using HOMER pro," Mater. Today Proc., no. February 2022, 2020.

[34] F. Pande, H. Thakre, S. Ladukar, and P. D. Radke, "Designing and Optimizing a Hybrid Renewable System Using Homer for Site Selected," IJSRSET, vol. 3, no. 2, pp. 165–170, 2017.

[35] N. K. R. Md.Nurunnabi, "Grid Connected Hybrid Power System Design Using HOMER," in Proceedings of 2015 3rd International Conference on Advances in Electrical Engineering, 2018, no. November.

[36] [36] P. Gilman and P. Lilienthal, "MICROPOWER SYSTEM MODELING." National Renewable Energy Laboratory 15.1, pp. 379–418.

[37] A. Ramseebaluck, "Hybrid Renewable-based Reliable and Cost-effective Rural Electrification in Southern Africa," in The 10th International Renewable Energy Congress (IREC 2019) Hybrid, 2019, no. Irec.

[38] Z. Zhang et al., "Short-term optimal operation of wind-solar-hydro hybrid system considering uncertainties," Energy Convers. Manag., vol. 205, no. October 2019, p. 112405, 2020.

[39] J. Mahmoudimehr and M. Shabani, "Optimal design of hybrid photovoltaic-hydroelectric standalone energy system for north and south of Iran," Renew. Energy, vol. 115, pp. 238–251, 2018.

[40] J. Jurasz, P. B. Dąbek, B. Kaźmierczak, A. Kies, and M. Wdowikowski, "Large scale complementary solar and wind energy sources coupled with pumped-storage hydroelectricity for Lower Silesia (Poland)," Energy, vol. 161, pp. 183–192, 2018.

[41] N. Guerra, M. Guevara, C. Palacios, and F. Crupi, "Operation and physics of photovoltaic solar cells : an overview Operation and physics of photovoltaic solar cells : an overview Funcionamiento y física de celdas solares fotovoltaicas : una visión general," no. December, 2018.

[42] A. Ameur, A. Berrada, K. Loudiyi, and R. Adomatis, Performance and energetic modeling of hybrid PV systems coupled with battery energy storage. Elsevier Inc., 2021.

[43] S. Dorji, D. Wangchuk, T. Choden, and T. Tshewang, "Materials Today : Proceedings Maximum Power Point Tracking of solar photovoltaic cell using Perturb & Observe and fuzzy logic controller algorithm for boost converter and quadratic boost converter," Mater. Today Proc., vol. 27, pp. 1224–1229, 2020.

[44] S. Vijiyasamundiswary and P. S. Kumar, "Reliability and Cost Analysis of," 2013 Int. Conf. Comput. Power, Energy, Inf. Commun., pp. 84–88, 2013.

[45] E. Skoplaki, A. G. Boudouvis, and J. A. Palyvos, "A simple correlation for the operating temperature of photovoltaic modules of arbitrary mounting," Sol. Energy Mater. Sol. Cells, vol. 92, no. 11, pp. 1393–1402, 2008.

[46] J. Jurasz, J. Mikulik, M. Krzywda, B. Ciapała, and M. Janowski, "Integrating a wind- and solar-powered hybrid to the power system by coupling it with a hydroelectric power station with pumping installation," Energy, vol. 144, pp. 549–563, 2018.

[47] T. F. Fofang, "Design and Simulation of Off-Grid Solar / Mini- H ydro Renewable Energy System using Homer Pro Software : Case of Muyuka Rural Community," Int. J. Eng. Res. Technol., vol. 9, no. 09, pp. 597–604, 2020.

★★★